# Reevaluating UMa3/U1: Star Cluster or the Smallest Known Galaxy?

Scot Devlin,[1]★ Holger Baumgardt,[1] Sarah Sweet[1,2]
[1]School of Mathematics and Physics, The University of Queensland, St. Lucia, QLD 4072, Australia
[2]ARC Centre of Excellence for All Sky Astrophysics in 3 Dimensions (ASTRO 3D), Australia

Accepted XXX. Received YYY; in original form ZZZ

**ABSTRACT**

Ursa Major III/UNIONS 1 (UMa3/U1), the smallest and faintest Milky Way satellite discovered to date, exhibits an absolute V-band magnitude of $+2.2 \pm 0.4$ and a half-light radius of $3 \pm 1$ pc. While its true nature remains uncertain pending multi-epoch spectroscopic data, Errani et al. (2024) suggest that UMa3/U1 is a dwarf galaxy. This conclusion is based on its large velocity dispersion and the improbability, as indicated by dynamical cluster simulations, of its long-term survival if it were a dark matter-free star cluster.

We model the evolution of UMa3/U1 as a star cluster using collisional N-body simulations to find that it would have a remaining lifetime of $2.4\,\mathrm{Gyr} \pm 0.3\,\mathrm{Gyr}$, thereby allowing for the possibility that UMa3/U1 is a star cluster. The findings show a significant difference in the observable mass functions between UMa3/U1 star cluster and galaxy models, with a p-value $\ll 1$, but no convincing difference in observable mass segregation. Therefore, it is suggested that future observations should target the mass function as a classifier for UMa3/U1 and other very small Milky Way satellites of uncertain nature.

**Key words:** Cold dark matter (265); Dwarf spheroidal galaxies (420); Low surface brightness galaxies (940); the Milky Way (1054); N-body simulations (1083); Star clusters (1567); Tidal disruption (1696)

## 1 INTRODUCTION

Dwarf galaxies and star clusters are of significant cosmological interest. Globular clusters, a type of star cluster, are believed to be ancient systems that have not undergone substantial chemical enrichment, making them valuable probes of the interstellar medium at the time of their formation (Krumholz et al. 2019). Dwarf galaxies are an excellent dark matter probe, particularly at the smallest scales, because they contain just enough visible matter to trace the distribution of invisible dark matter, without having so much visible matter that it significantly contributes to the total galaxy mass. This is particularly true for the smallest dwarf galaxies, known as ultrafaint dwarf galaxies (UFDs). UFDs provide crucial insights into the minimum dark matter halo mass required for galaxy formation (Bode et al. 2001). Additionally, the absolute number of UFDs places constraints on the mass of the dark matter particle (Simon 2019) and constrains star formation theories (Munshi et al. 2019). Being less influenced by baryonic processes than other galaxies, UFD density profiles provide valuable insights for testing cosmological models, making them key to research on the cusp-core problem Almeida et al. (2024).

Distinguishing between SCs and UFDs is an important task, especially given the rapid increase in the discovery of faint Milky Way satellites since the early 2000s with the advent of wide-field digital photometric surveys (Simon 2019). The more recent use of spectroscopic surveys and Gaia mission data has enabled observers to apply 3D and proper motion filters to enhance the identification of increasingly fainter Milky Way satellites, even in the presence of poor 2D photometric data.

Before the 21st century, galaxies were distinguished from star clusters primarily by their size. A group of stars was classified as a galaxy if it was very large, and as a cluster if it was small. Even up until as recent as 2019, when observing stellar systems brighter than $M_V \approx -5$ in the Milky Way halo, a clear size distinction between globular clusters and dwarf galaxies remained; all globular clusters had a half-light radius of less than 20 pc, whereas all galaxies had a half-light radius greater than 100 pc (Simon 2019). But for fainter stellar systems the magnitude-size plane has been and continues to be useful, as globular clusters are known to be more compact for their luminosity, see Figure 2 of Simon (2019), Figure 9 of Smith et al. (2024), and Figure 6 of Baumgardt et al. (2022). With the discovery of many faint systems by wide-field photometric surveys like SDSS and Pan-STARRS in the mid-2000s, the magnitude-size plane became increasingly crowded at the faint end. This overlap made it more challenging to distinguish between star clusters and dwarf galaxies based solely on their radii and luminosities, prompting the need for additional classification criteria.

In addition to having a dynamical mass much larger than their baryonic mass—reflected in their high mass-to-light ratios of $M/L \sim 10^3 \left(\frac{M_\odot}{L_\odot}\right)$ (Simon 2019), compared to the very low mass-to-light ratios of star clusters ($1.4 < M/L_V < 2.5$) (Baumgardt et al. 2020)—UFDs are distinguished from star clusters by their non-zero spread in metallicities (Willman et al. 2011). The deeper gravitational well provided by the dark matter halo increases the velocity dispersion, enabling UFDs to better retain supernova remnants,

★ E-mail: s.devlin@uq.edu.au

which facilitates extended star formation histories and elemental self-enrichment.

The recently identified Ursa Major III/UNIONS 1 (UMa3/U1 or U1 if referring to the system as a star cluster and UMa3 if referring to the satellite as a Ultra Faint Dwarf galaxy), discovered through the deep, wide-field Ultraviolet Near Infrared Optical Northern Survey (UNIONS), is the least luminous known satellite of the Milky Way. It has an absolute V-band magnitude of $M_V = 2.2^{+0.3}_{-0.4}$ and is located at a heliocentric distance of $10 \pm 1$ kpc (Smith et al. 2024). It is 1.5 magnitude fainter than the next faintest Milky Way satellites, notably the ultrafaint dwarfs Kim 3 ($M_V = +0.7$ mag; Kim et al. 2016) and DELVE 5 ($M_V = +0.4$ mag; Cerny et al. 2023). Its small size, with a half-light radius of $R_h = 3 \pm 1$ pc, falls within the size range of known globular clusters but is an order of magnitude smaller than the smallest confirmed ultra-faint dwarf galaxy, Willman 1, which has a half-light radius of approximately $R_h \approx 20$ pc (Willman et al. 2011).

The faintest confirmed UFD's are fainter than the faintest globular clusters, so Uma3/U1 would more likely extend the UFD luminosity range, but it's size is within the current size range of confirmed globular clusters. The high velocity dispersion, $\sigma_{los} = 3.7^{+1.0}_{-1.4}\,\mathrm{km\,s^{-1}}$ (Smith et al. 2024) observed in UMa3/U1 suggests that it is a dark matter-dominated galaxy. If it were a self-gravitating star cluster devoid of dark matter, its velocity dispersion would be expected to be about 50 m/s. Errani et al. (2024) uses the parameters estimated by Smith et al. (2024) ($M_* = 16^{+6}_{-5}\,M_\odot$ and $R_h = 3 \pm 1\,\mathrm{pc}$) and the projected virial theorem formula for a cluster with a spherical exponential density profile to obtain a line-of-sight velocity dispersion of $\sigma_{los} = 49^{+14}_{-11}$ m/s.

The total mass of a dispersion-supported star system can be reliably constrained by velocity dispersion only if three key assumptions are met: the system is in dynamical equilibrium, contamination by binary stars is minimal, and contamination by foreground and background stars is negligible (Simon 2019). While foreground, background, and tidally unbound stars can be largely filtered out using isochrone methods, accurately identifying binary stars requires multi-epoch spectroscopic surveys with appropriate cadence. McConnachie & Côté (2010) find that unidentified binaries do not significantly increase the velocity dispersion of globular clusters beyond about 4.5 km/s. For larger UFDs and most substantial star clusters, the impact of a few binaries on overall velocity dispersion is minimal (Simon 2019). However, with only 11 likely member stars (Smith et al. 2024), UMa3/U1 is far more susceptible to artificial inflation of velocity dispersion due to small number statistics. Smith et al. (2024) note this issue, and show that the removal of the star with the largest outlying velocity would result in $\sigma_{los} = 1.9^{+1.4}_{-1.1}\,\mathrm{km\,s^{-1}}$, still large enough to constitute a dynamical mass 3 orders of magnitude larger than the stellar mass, when using the dynamical half mass found in Wolf et al. (2010):

$$M_{1/2} = 930 \left(\frac{\sigma}{\mathrm{km\ s^{-1}}}\right)^2 \left(\frac{R_{1/2}}{\mathrm{pc}}\right) M_\odot \tag{1}$$

where $\sigma$ is the velocity dispersion and $R_{1/2}$ is the projected two-dimensional half-light radius. Removing the second largest outlier results in a formally unresolved velocity dispersion, consistent with what would be expected if UMa3/U1 is a self-gravitating star cluster.

Errani et al. (2024) argue that if UMa3/U1 were a star cluster, its low density would cause it to quickly disintegrate due to tidal interactions with the Milky Way's gravitational potential. Using the collisionless particle mesh code, SUPERBOX (Fellhauer et al. 2000), they demonstrate that UMa3/U1 could not survive more than 0.4 Gyr as a dark matter free star cluster. Since this is short compared to its proposed $\approx$ 12 Gyr age (Smith et al. 2024), observing UMa3/U1 just before its demise is unlikely. Thus, they conclude UMa3/U1 is more likely a UFD protected from tidal stripping by its own dark matter halo. In this paper, we present collisional modeling of the tidal evolution of UMa3/U1 as a star cluster, demonstrating that when interstellar forces and stellar evolution are taken into account, UMa3/U1, though heavily stripped by Milky Way tidal forces, survives for a longer period of time.

Consequently, the question of whether UMa3/U1 is a star cluster or an ultra-faint dwarf galaxy remains open until multi-epoch spectroscopy can confirm its high velocity dispersion. We also look at two alternate ways of differentiating star clusters from UFDs, and apply them to our U1 models: stellar mass segregation (Baumgardt et al. 2022), and present day mass function. We believe we are the first to propose the present-day mass function as a distinguishing property for differentiating between ultra-faint dwarf galaxies and star clusters.

The work is presented as follows: Section 2 describes the method used to model UMa3/U1 as a star cluster. Section 3 explains how the model velocity dispersions are calculated and compares these results to analytical velocity dispersion values. Section 4 discusses the results for U1's time to dissolution, comparing them to previous published results, and comments on the implications for the identity of UMa3/U1. Section 5 presents the mass segregation of the model cluster, and discusses its usefulness in classifying UMa3/U1. Section 6 describes the method and rationale for modeling the present-day mass function of UMa3 and U1, and discusses the usefulness of the mass function as a parameter for classifying UMa3/U1, as well as other faint Milky Way satellites. The results and conclusions are summarized in Section 7, and the limitations of our methods are discussed in Section 8.

## 2 N-BODY SIMULATIONS

The simulations were carried out with the collisional Aarseth N-body code NBODY7 (Nitadori & Aarseth 2012). The code uses a Hermite scheme with individual time-steps for the integration and handles close encounters between stars using KS (Kustaanheimo & Stiefel 1965) and chain regularizations (Mikkola & Aarseth 1989, 1993). Our simulations modeled stellar evolution by fitting the formulae of Hurley et al. (2000), which provide stellar lifetimes, luminosities, and radii as functions of initial mass and metallicity for all phases of stellar evolution, from the zero-age main sequence to the remnant stages.

### 2.1 Cluster Orbit and Milky Way Potential

To understand how long UMa3/U1 will survive if it is a cluster, it is necessary to simulate the effects of tidal stripping and stellar evolution on U1 from the cluster's birth. While NBODY7 can precisely calculate the effects of tidal stripping by tracking the cluster's position relative to the Milky Way over time, the initial position and velocity of the cluster relative to the Milky Way potential are required to begin the simulation. This ensures that the simulation accurately tracks the effects of tidal stripping throughout the cluster's lifetime. This was done by taking the six phase-space coordinates describing UMa3/U1's present-day position and motion, as provided in Table 3 of Smith et al. (2024), and utilising the program Galpy (Bovy 2015) to integrate a mass-less test particle backwards under the influence of the Bovy (2015) Milky Way potential, as detailed in Section 2.1, for a duration of 12 Gyr. To convert from equatorial to Galactic

Cartesian coordinates, we employed the solar velocity relative to the Local Standard of Rest (LSR) from Schönrich et al. (2010), assuming a solar distance to the Galactic center of 8 kpc, a solar height above the Galactic plane of 0 pc, and a circular velocity of the LSR around the Galactic center of 220 km/s. This provided the starting position and velocity for the N-body simulation: $x = 17.404$ kpc, $y = -19.215$ kpc, $z = -19.285$ kpc, and velocities $U = 20.418$ km/s, $V = 141.333$ km/s, and $W = 10.903$ km/s.

We utilize the Milky Way potential from Bovy (2015) for both determining our model cluster's initial position and for the potential in our n-body simulations. This potential includes contributions from a thin disk, thick disk, bulge, and halo. Both the thin and thick disks are modeled as axisymmetric exponential disks. The thin disk has a surface density at the solar radius of $\Sigma_0 \approx 870\,M_\odot\,\mathrm{pc}^{-2}$, a scale length of $R_d \approx 2.6$ kpc, and a scale height of $z_d \approx 0.3$ kpc (Miyamoto & Nagai 1975). The thick disk has a surface density of $\Sigma_{0,\mathrm{thick}} \approx 220\,M_\odot\,\mathrm{pc}^{-2}$, a scale length of $R_{d,\mathrm{thick}} \approx 2.0$ kpc, and a scale height of $z_{d,\mathrm{thick}} \approx 0.9$ kpc (Miyamoto & Nagai 1975). The bulge is described by a Hernquist profile, with a bulge mass of $M_b \approx 1.5 \times 10^{10}\,M_\odot$ and a scale radius of $a_b \approx 0.6$ kpc (Hernquist 1990). The halo is modeled using a Navarro-Frenk-White (NFW) profile, with a halo mass of $M_h \approx 10^{12}\,M_\odot$ and a scale radius of $r_s \approx 20$ kpc (Navarro et al. 1997).

### 2.2 Replicating the UNIONS observatory

The Pan-STARRS observatory has a saturation limit of $i = 17.5$ mag and achieves a median $5\sigma$ point-source depth of $i = 24.0$ mag, from which Smith et al. (2024) adopt a completeness limit of 23.5 mag. All Smith et al. (2024) i-band work is specifically from the Pan-STARRS i-band catalogs.

We estimate which stars the UNIONS observatory would observe in our model U1 by creating a filter for our models hereafter referred to as the 'UNIONS range.' The UNIONS range filters out: (a) stars fainter than the adopted completeness limit of apparent i-band magnitude $i = 23.5$ mag and stars brighter than the saturation limit of $i = 17.5$ mag (Smith et al. 2024); (b) stellar remnants; and (c) stars that are not located within an ellipse centered on the density center, with a semi-major axis of four times the half-light radius ($4 \times r_h = 12$ pc) and an ellipticity of $\epsilon = 0.5$ (Table 2 of Smith et al. 2024).

We performed the UNIONS range (a) filter by excluding stars with masses higher than $0.792\,M_\odot$ and lower than $0.305\,M_\odot$, the mass equivalents to 17.5 and 23.5 in apparent i-band magnitude as measured by the Pan-STARRS observatory. To obtain the conversion from apparent i-band magnitudes to equivalent masses, we used the Padova and Trieste Stellar Evolution Code (PARSEC) 1.2 track isochrones (Bressan et al. 2012), utilizing the CMD 3.7 tool to find the best-matched isochrone to the following parameters:

(i) An extinction of $A_v = 0.0584$ from a color excess $E(B-V) = 0.0213$, obtained using the extinction tool, GALExtin (Amôres et al. 2021), employing the Schlegel et al. (1998) extinction map, and inputting the locations of UMa3/U1 from Smith et al. (2024)

(ii) A metallicity of $Z = 0.0001$ (rounded up from 0.0000959 because PARSEC isochrones are only listed down to $Z = 0.0001$), equivalent to the $[Fe/H] = -2.2$ of UMa3/U1 found by Smith et al. (2024) when solar $Z = 0.0152$, and assuming the Fe proportion scales with the total metals proportion.

(iii) A 12 Gyr age from Smith et al. (2024).

### 2.3 Modelling the UMa3/U1 progenitor

The models used for the progenitors assumes U1 to have been spherically symmetric, with an isotropic velocity distribution and no primordial mass segregation. The models are created using a program as described in Hilker et al. (2007). We assume a Kroupa (2001) like initial mass function (IMF) defined by Baumgardt et al. (2023). It has a three-stage power law with a near-Salpeter-like (Salpeter 1955) slope above 1.0 $M_\odot$, a shallower slope below 0.4 $M_\odot$, and an intermediate slope between 0.4 and 1.0 $M_\odot$:

$$\xi(m)\,dm \sim \begin{cases} m^{-0.3}\,dm, & \text{for } m < 0.4\,M_\odot \\ m^{-1.65}\,dm, & \text{for } 0.4\,M_\odot \le m < 1.0\,M_\odot \\ m^{-2.3}\,dm, & \text{for } m \ge 1.0\,M_\odot \end{cases}$$

The progenitors start with a physical half-light radius, $r_{h,phys} = 3$ pc (equal to the current physical half-light radius observed for UMa3/U1 by Smith et al. (2024)), a King (1962) model concentration parameter of $c = 1$, and a metallicity of $Z = 0.0001$ (see Section 2.2). The Hilker et al. (2007) program deprojects the King (1962) density profile given by these structural parameters into a 3-dimensional density profile using Abel's integral equation. It then calculates the cumulative mass function $M(< r)$ and the potential energy $\phi(r)$ from the 3-dimensional density profile. From these, the energy distribution function $f(E)$ is calculated with the help of Eqs. (4)-140a from Binney & Tremaine (1987), assuming isotropic orbits for the stars. It then creates an N-body representation using the deprojected density profile and the distribution function. The program outputs initial $x$, $y$, and $z$ positions, as well as $v_x$, $v_y$, and $v_z$ velocities for all stars.

To choose the progenitor size, $n$, we conducted multiple trial N-body integrations, starting from the positions and velocities listed in Section 2.1, varying the number of stars in the progenitor cluster, $n$, between 1,000 and 30,000 while keeping $r_{h,\mathrm{phys}}$, $c$, and $Z$ constant at the values mentioned above. The progenitor size, $n$, for the simulations to be analyzed was selected by identifying the trial simulation that came closest to 12 Gyr with 21 stars (the mean number of stars in the mock UMa3/U1 populations of Smith et al. (2024)) remaining in the UNIONS range.This was done for a 0.0 black hole and neutron star retention fraction and a 0.1 black hole and neutron star retention fraction. These retention rates were chosen because the relatively small mass of our starting cluster dictates escape velocity of about 4-5 km/s. This low escape velocity is below the modeled neutron star natal kick velocity found across most remnant masses for the majority of different asymmetric supernova mechanisms (Figure 11 in Banerjee et al. (2020)). It was found that the progenitor of UMa3/U1 should have n=6000 stars if all black holes and neutron stars are given natal kick velocity's above the escape velocity, and n=7200 if 90% of the black holes and neutron stars are given natal kick velocity's above the escape velocity.

We modeled multiple clusters with a 0.0 retention fraction and $n = 6000$ stars until we obtained ten simulations that matched the 21 star size of U1 in the UNIONS range, within a time-frame between 10 Gyr and 14 Gyr. The same procedure was was performed for clusters with a 0.1 retention fraction and $n = 7200$ stars. The results of the twenty simulations are shown in table 1.

Although none of the simulations with a a 0.0 retention fraction reached n=21 in UNIONS range at exactly 12 Gyr, all runs came consistently close to this mark, so the first ten runs were used for analysis. The clusters with a a 0.1 retention fraction exhibited greater variability in their lifetimes and the time to reach 21 stars due to the more unpredictable nature of clusters with more remnants. In these simulations, it was common for the disruption of a single black hole binary to lead to the rapid dissolution of the cluster, with the

timing of such events being stochastic (Figure 3) . Consequently, 19 simulations were conducted to obtain 10 that fell within the desired time window of 10 to 14 Gyr.

### 2.4 Bound Star Method: Tidal Radius and Density Centre Calculations

To understand how many stars remain bound in the cluster at a particular time in the simulations the density centre is determined using the method of Casertano & Hut (1985), calculating the local density around each star by taking the inverse cube of the distance to the 7th nearest neighbour. For the tidal radius we use the formulae for spherically symmetric isothermal potentials of constant rotation velocity:

$$r_t = \left(\frac{GM_c}{2V_G^2}\right)^{1/3} R_G^{2/3} \tag{2}$$

where $M_c$ is the mass of the cluster, $V_G$ is the circular velocity of the Galaxy, and $R_G$ is the distance of the cluster from the Galactic Centre. For the eccentric orbit of UMa3/U1 we set $V_G$ to be the instantaneous orbital velocity and $R_G$ to be the instantaneous distance from UMa3/U1 to galaxy centre. Thus the tidal radius for each time step is calculated. Because an accurate cluster lifetime relies on an accurate time of complete dissolution, it is necessary to capture the last moments of the clusters life. In some simulations the cluster survives with less than 8 stars for 100+ Myr. In these cases the Casertano & Hut (1985) method was adjusted at the time steps where less than 8 stars were bound to take the inverse cube of the distance to the 6th, 5th, or 4th nearest neighbour of each bound star, thereby allowing the desnity centre to compute for smaler cluster sizes later in time.

The initial Mass of the cluster, $M_c$ includes all stars in the cluster progenitor model, and all stars are assumed 'bound'. Subsequent time steps initially calculate the density centre and cluster mass, $M_c$ from the current position and mass of all the bound stars of the previous time step. $R_G$ is then calculated from the new density centre, and a new tidal radius is found. The new tidal radius is used to create a 3D filter in the shape of a sphere of radius = $r_t$, with any star outside of the sphere considered unbound. We then update our density centre, $M_c$ and $R_G$ using only the new set of bound stars. This iteration loop continues until conversion.

## 3 VELOCITY DISPERSION

At the start of each simulation, clusters did not contain binaries. Binaries and higher-order hierarchies that formed during the integration were treated as inert, by assuming that no collisions or exchange of mass take place and that the stellar evolution of the components is not altered by their companions.

We calculate a aggregate velocity dispersion for U1 by taking the component velocities of the stars in the UNIONS range, $V_x$, $V_y$, and $V_z$ and concatenating them in a list and then taking the standard deviation of that list as the velocity dispersion of the cluster.

The velocity dispersion of each simulation can be found in tables 1 and 2. In these tables, the following symbols and units are used: $s$ refers to the simulation number, $T_{\rm diss}$ (Myr) represents the dissolution time in million years, $\sigma_{\rm all}$ (km/s) indicates the velocity dispersion of all bound stars in kilometers per second, $\sigma_{\rm HST}$ (km/s) denotes the velocity dispersion of stars except remnant stars (simulating deep photometry) in kilometers per second, and $\sigma_{\rm U}$ (km/s) stands for the velocity dispersion of stars observable by UNIONS in kilometers per second. $P_{\rm PDMF}$ (HST) refers to the p-value of the present-day mass function for all stars except remnant stars, while $KS_{\rm PDMF}$ (HST) indicates the KS statistic of the present-day mass function for all stars except remnant stars. $P_{\rm PDMF}$ (Unions) describes the p-value of the present-day mass function for what the UNIONS observatory would see, and $KS_{\rm PDMF}$ (Unions) shows the KS statistic of the present-day mass function for what the UNIONS observatory would see. $\rho_e$ (all) ($M_\odot$ kpc$^{-3}$) measures the density of all bound stars in the half-light radius in solar masses per cubic kiloparsec, and $\rho_e$ (HST) ($M_\odot$ kpc$^{-3}$) represents the density of all stars except remnant stars in the half-light radius in solar masses per cubic kiloparsec.

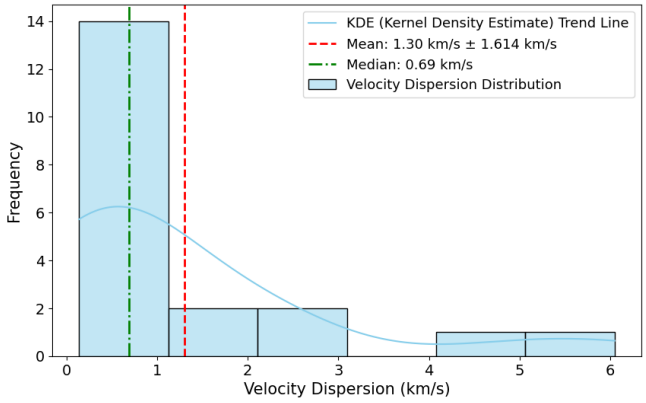


**Figure 1.** Distribution of velocity dispersion values of all simulations at the Uma3/U1 size of n=21 stars in the UNIONS range. The blue line is the kernel density estimate trend line.

The velocity dispersion of the twenty star clusters observed within the UNIONS range, at the specified UNIONS size of 21 stars, has a mean of 1.298 km/s with a standard deviation of ± 1.614 km/s. Given the non-normal distribution of the data (see Figure 1), additional non-parametric measures were also considered: the median velocity dispersion was found to be 0.694 km/s, with an interquartile range of 1.547 km/s.

### 3.1 Velocity Dispersion Discussion

For a spherically symmetric cluster in dynamical equilibrium with a isotropic velocity distribution, the full velocity dispersion can be estimated from the virial theorem to be:

$$\sigma = \sqrt{\frac{GM}{5r_h}} \tag{3}$$

where G is the gravitational constant, M is the mass of the cluster and $r_h$ is the half light radius. Using $G = 4.30 \times 10^{-3}$ pc $M_\odot^{-1}$ (km/s)$^2$, the mean mass of the twenty model U1 star clusters, $M = 146.84\ M_\odot$ and the mean half-light radius of the twenty U1 star clusters $r_h = 3.39$ pc, gives a velocity dispersion of $\sigma = 37.3$m/s, equivalent to a line of sight velocity of $\sigma_{\rm los} = \frac{\sigma}{\sqrt{3}} = 21.5$m/s which is within an order of magnitude of the line of sight velocity dispersion estimate for U1 from Errani et al. (2024): $\sigma_{los} = 49^{+14}_{-11}$.

We are confident that our bound star method (2.4) effectively excludes foreground and background stars. Therefore the significantly inflated velocity dispersion's observed in our simulations (Figure 1), compared to our and Errani et al. (2024)'s analytical velocity dispersion estimates, indicate that binary stars greatly inflate the velocity

**Table 1.** Results for 0.1 BH Retention Simulations

| s | $T_{\rm diss}$ (Myr) | $\sigma_{\rm all}$ (km/s) | $\sigma_{\rm HST}$ (km/s) | $\sigma_{\rm U}$ (km/s) | $P_{\rm PDMF}$ (HST) | $KS_{\rm PDMF}$ (HST) | $P_{\rm PDMF}$ (Unions) | $KS_{\rm PDMF}$ (Unions) | $\rho_e$ (all) ($M_\odot$ kpc$^{-3}$) | $\rho_e$ (HST) ($M_\odot$ kpc$^{-3}$) |
|---|---|---|---|---|---|---|---|---|---|---|
| 1 | 2380 | 1.753 | 1.746 | 1.746 | 1.33E-09 | 0.273 | 0.218 | 0.318 | 2.96E+08 | 2.72E+07 |
| 2 | 840 | 0.656 | 0.593 | 0.618 | 8.03E-08 | 0.255 | 0.095 | 0.381 | 5.47E+08 | 4.36E+07 |
| 3 | 120 | 0.960 | 0.151 | 0.139 | 1.50E-08 | 0.327 | 0.196 | 0.333 | 3.60E+08 | 4.35E+07 |
| 4 | 220 | 2.163 | 2.185 | 2.216 | 1.11E-01 | 0.273 | 0.365 | 0.286 | 3.57E+08 | 3.23E+07 |
| 5 | 1680 | 2.436 | 2.435 | 2.430 | 9.65E-09 | 0.200 | 0.001 | 0.600 | 2.44E+08 | 2.41E+07 |
| 6 | 1880 | 0.155 | 0.166 | 0.177 | 1.82E-07 | 0.509 | 0.000 | 0.619 | 5.61E+08 | 9.88E+07 |
| 7 | 2740 | 0.918 | 0.204 | 0.202 | 7.99E-07 | 0.273 | 0.007 | 0.500 | 3.74E+08 | 1.70E+07 |
| 8 | 1559 | 0.247 | 0.191 | 0.182 | 2.88E-04 | 0.327 | 0.016 | 0.476 | 2.10E+08 | 2.56E+07 |
| 9 | 1600 | 0.484 | 0.339 | 0.344 | 7.12E-06 | 0.091 | 0.049 | 0.409 | 2.67E+08 | 4.09E+07 |
| 10 | 4560 | 0.770 | 0.376 | 0.375 | 2.25E-06 | 0.409 | 0.005 | 0.524 | 3.63E+08 | 3.06E+07 |

**Table 2.** Results for 0.0 BH Retention Simulations

| s | $T_{\rm diss}$ (Myr) | $sigma_{\rm all}$ (km/s) | $sigma_{\rm HST}$ (km/s) | $sigma_{\rm U}$ (km/s) | $P_{\rm PDMF}$ (HST) | $KS_{\rm PDMF}$ (HST) | $P_{\rm PDMF}$ (Unions) | $KS_{\rm PDMF}$ (Unions) | $\rho_e$ (all) ($M_\odot$ kpc$^{-3}$) | $\rho_e$ (HST) ($M_\odot$ kpc$^{-3}$) |
|---|---|---|---|---|---|---|---|---|---|---|
| 01 | 2080 | 5.985 | 6.019 | 6.047 | 5.00E-06 | 0.634 | 0.365 | 0.286 | 3.996E+08 | 4.014E+07 |
| 02 | 2220 | 0.304 | 0.277 | 0.307 | 5.01E-12 | 0.720 | 0.603 | 0.238 | 9.019E+08 | 1.067E+08 |
| 03 | 2361 | 1.025 | 0.927 | 0.920 | 1.26E-10 | 0.704 | 0.041 | 0.429 | 3.682E+08 | 4.650E+07 |
| 04 | 2799 | 4.889 | 4.915 | 4.923 | 3.06E-09 | 0.703 | 0.002 | 0.571 | 4.312E+08 | 5.368E+07 |
| 05 | 2140 | 0.165 | 0.184 | 0.199 | 1.99E-07 | 0.632 | 0.196 | 0.333 | 4.660E+08 | 6.531E+07 |
| 06 | 2160 | 0.940 | 0.942 | 0.962 | 2.34E-04 | 0.489 | 0.005 | 0.524 | 5.829E+08 | 6.106E+07 |
| 07 | 2480 | 0.433 | 0.425 | 0.426 | 2.95E-07 | 0.636 | 0.041 | 0.429 | 3.285E+08 | 5.581E+07 |
| 08 | 2820 | 2.061 | 2.084 | 2.072 | 8.01E-05 | 0.528 | 0.005 | 0.524 | 3.348E+08 | 6.439E+07 |
| 09 | 2939 | 0.786 | 0.775 | 0.769 | 6.72E-08 | 0.638 | 0.016 | 0.476 | 3.456E+08 | 3.847E+07 |
| 010 | 2260 | 0.868 | 0.891 | 0.905 | 7.73E-06 | 0.560 | 0.016 | 0.476 | 3.906E+08 | 3.445E+07 |

dispersion of UMa3/U1. The measured velocity dispersion by Smith et al. (2024) falls well within the range of our cluster model dispersion's (Figure 1): 10% of our models exceed the UMa3/U1 member star velocity dispersion measured by Smith et al. (2024) 3.7 km s$^{-1}$, and 25% exceed 1.9 km s$^{-1}$, the velocity of UMa3/U1 when the largest velocity outlier is excluded.

It's important to note that these models are made with no primordial binary's, thus the velocity dispersion's may be underestimated, further highlighting the possibility that the measured velocity dispersion found by Smith et al. (2024) is inflated by binary's. This confirms the necessity of multi-epoch spectroscopy in order to obtain a velocity dispersion that accurately reflects the mass-to-light ratio of UMa3/U1.

## 4 TIME TO DISSOLUTION

The time to dissolution for each simulation analysed can be found in tables 1 and 2. Figure 2 shows the distribution of times to dissolution from UNIONS stars in the UNIONS range. Whilst both distributions look non normal, both satisfy the Shapiro & Wilk (1965) normal distribution test, so we report only the mean with standard deviation: For the ten simulations with a 0.1 retention rate: $\bar{x} = 1758 Myr \pm$ 1299Myr and for the ten with a 0.0 retention rate $\bar{x} = 2426 Myr \pm$ 317Myr. The 0.0 retention simulations exhibit less variability in the time to dissolution. This reduced variability is attributed to the rapid dissolution of the cluster once a central black hole binary breaks up, as well as the variability in the black hole binary masses and lifetimes. An example can be seen in Figure 3: simulation 2 has a large black hole binary which gets disrupted at 11740 Myr, causing a significant and rapid drop in the cluster's binding energy. As a result, the binding energy of the cluster falls below the kinetic energy of many stars, leading to their ejection from the cluster; the number of all bound stars decreases from 42 to 13 within 20 Myr, and the cluster survives only 80 Myr longer. In contrast, simulation 7, despite experiencing disruptions at earlier times, has a last remaining black hole binary with a longer lifetime. This allows the cluster to enter a more regular tidal stripping regime by the time it reaches UNIONS size (21 stars). This results in a slower decay and a significantly longer time to dissolution.

### 4.1 Time to Dissolution: Conclusion

Errani et al. (2024) posits that the globular cluster U1 could not survive in the Milky Way tidal field for much longer than a single orbit, which he estimates to be approximately 400 Myr. Our findings indicate that the average lifetime of U1 is significantly longer, exceeding 1.6 Gyr, which is over four times Errani's initial estimate. This discrepancy highlights the critical need for accurately calculating the forces between stars using collisional N-body simulations and for determining mass loss with stellar evolution models when estimating the survival time of a globular cluster in a gravitational potential. Assuming the collisisonal n-body simulations are more representative of the fate of U1, it is more likely that U1 would be a cluster visible to us today. Therefore we conclude UMa3/U1 may still be a star cluster.

We choose to headline the time to dissolution of the 0.0 retention simulations for several reasons. While supernova theory suggests that some natal kick mechanisms might be more symmetric at certain masses, resulting in velocities below the UMa3/U1 escape velocity of approximately 4-5 km/s (Fryer et al. 2012; Banerjee et al. 2020),

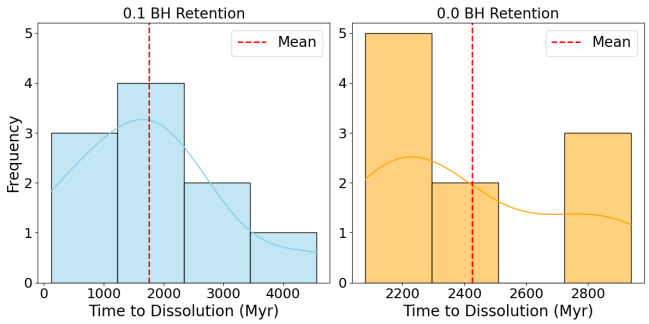


**Figure 2.** Left hand side: Distribution of the times to dissolution of the ten simulations with a 0.1 black hole retention fraction. Right hand side: Distribution of the times to dissolution of the ten simulations with a 0.0 black hole retention fraction. The blue and yellow lines, are kernel density estimate trend lines.

observations of neutron stars and black holes with such low velocities have not been made. Studies like Hobbs et al. (2005) indicate that the frequency of such low velocities should be expected to be less than 1%. Additionally, selection effects may have been introduced in the 0.1 simulations because the first 10 simulations did not all meet the required criteria of UNIONS size (21 stars) in the UNIONS range at 10 to 14 Gyr. Out of the nineteen runs needed, seven fell below 10 Gyr and only two exceeded 14 Gyr.

## 5 MASS SEGREGATION

Baumgardt et al. (2022) conducted a comprehensive analysis of over 50 globular clusters (GCs) and ultrafaint dwarf galaxies (UFDs), revealing that GCs with ages equal to or exceeding their relaxation times exhibit significant mass segregation. Given that most GCs are older than their relaxation times, mass segregation is a common characteristic among them. In contrast, UFDs generally have much higher relaxation times and do not exhibit mass segregation. Consequently, they concludes that mass segregation serves as a valuable distinguishing criterion between globular clusters and UFDs.

To determine whether mass segregation should be expected in our model cluster U1, we estimate the relaxation times according to Spitzer (1987):

$$T_{\rm RH} = 0.138 \frac{\sqrt{M} r_h^{1.5}}{\sqrt{G}\langle m \rangle \ln(\gamma N)}, \quad (4)$$

where $M$ is the (stellar) mass of the system, $r_h$ the three-dimensional half-mass radius, $\langle m \rangle$ the average mass of stars, and $N$ is the number of stars. $\gamma$ is a constant in the Coulomb logarithm for which we assume $\gamma = 0.11$ (Giersz & Heggie 1994).

Both the 0.1 retention simulations and the 0.0 retention simulations have relaxation times much shorter than the $\approx$ 13 Gyr lifetime of the model U1 clusters and can therefore be considered relaxed (Baumgardt et al. 2022). The 0.1 retention U1 model clusters, having more gravitational energy, take slightly longer to relax, with relaxation times of $T_{\rm RH} \approx 30$ Myr, compared to the 0.0 retention U1 clusters, which have relaxation times of $T_{\rm RH} \approx 15$ Myr. It is therefore highly likely that U1 is mass segregated. However, proving mass segregation using the known stars within the UNIONS range is challenging due to the small number of observable stars. The limited sample size makes obtaining statistically significant results difficult, and the exclusion of heavy remnant stars significantly reduces the representation of more massive stars, thereby diminishing the observed mass segregation. To mitigate the problem of small number statistics and include stars of lesser mass, we assume that UMa3/U1 may be the target for a space telescope like the Hubble Space Telescope or the James Webb Space Telescope. These telescopes would allow us to observe main sequence stars down to nearly 0.1 solar masses, close to the hydrogen burning limit. We therefore re-analyse our simulations taking into account all main sequence stars and excluding only the compact remnants. Taking this set of stars (HST range), the median stellar mass is found, and an equal number of stars above and below the median mass are plotted on a cumulative number of stars vs distance from cluster centre plot. For comparison, the same is done for all bound stars (including remnants). To quantify mass segregation a Kolmogorov-Smirnov (KS) test is perfomed on the cumulative distributions of faint and bright stars to assess the significance of the differences between these distributions (Press et al. 1992).

**Table 3.** Mass segregation statistics for different retention runs at UNIONS time. 'all bound stars' = All stars in the simulation cluster, 'HST bound stars' = All stars in the simulation cluster except for remnants

| Retention Run | Metric | Average Value | Median | SIQR |
|---|---|---|---|---|
| 0.1 (all bound stars) | p-value | $0.1139 \pm 0.1729$ | 0.0270 | 0.0596 |
| | KS-stat | $0.2376 \pm 0.0665$ | 0.2259 | 0.0599 |
| 0.0 (all bound stars) | p-value | $0.0091 \pm 0.0250$ | 0.0003 | 0.0009 |
| | KS-stat | $0.3185 \pm 0.0599$ | 0.3226 | 0.0245 |
| 0.1 (HST bound stars) | p-value | $0.4484 \pm 0.3526$ | 0.4171 | 0.2615 |
| | KS-stat | $0.2738 \pm 0.1139$ | 0.2818 | 0.0486 |
| 0.0 (HST bound stars) | p-value | $0.4671 \pm 0.2651$ | 0.5275 | 0.1680 |
| | KS-stat | $0.2820 \pm 0.0625$ | 0.2632 | 0.0338 |

### 5.1 Mass Segregation: Results and Conclusion

An example of one of the mass segregation plots is shown in figure 4. It is clear form these cumulative distributions plots that mass segregation is apparent when looking at all bound stars, but most simulations within the HST range do not show clear mass segregation.

This is borne out by the KS tests, the KS-stat and p-values for which are found in Table 3. When including all bound stars both the 0.0 and 0.1 retention simulations show p-values close to the significance level of 0.05. Whereas the deep photometry stars, HST bound stars, consistently show a much lower significance with $p \ll 0.05$

We therefore conclude that if UMa3/U1 is a self gravitating star cluster, then it is likely mass segregated as its relaxation time is less than its age and our N-body simulations show mass segregation. But mass segregation is not currently a useful classification tool for UMa3/U1 because our N-body simulations show that the stars seen by deep photometry surveys do not display mass segregation to a significant level.

## 6 MASS FUNCTION

We evaluate the effectiveness of the mass function as a criterion for differentiating UFDs from star clusters by comparing the stacked mass profiles of ten simulations—0.0 retention and 0.1 retention—at UNIONS time (21 stars) in the HST range, against a modeled UMa3 mass profile assuming deep photometry. We find the stacked 0.0 retention simulations to have 374 stars in the HST range at UNIONS time, and the stacked 0.1 retention simulations to have 479 stars in

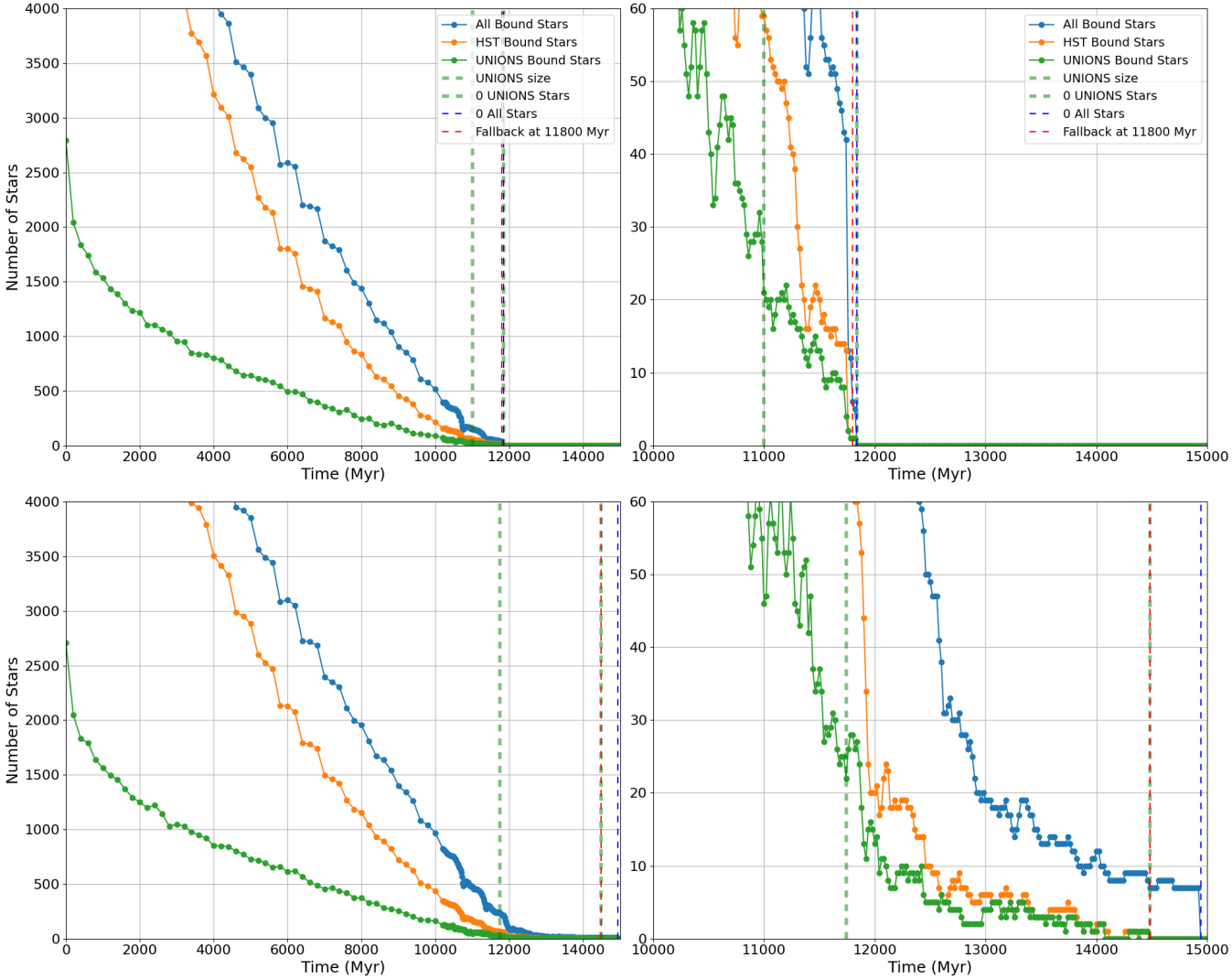


**Figure 3.** Time evolution from simulation 2 (top) and simulation 7 (bottom) in the 0.1 neutron star and black hole retention set.

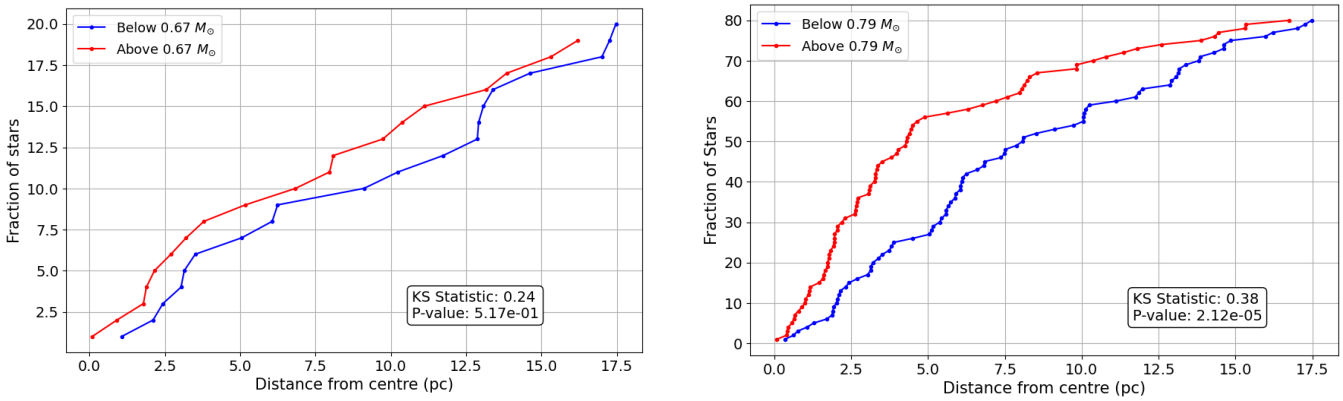


**Figure 4.** Mass segregation from simulation 03 in the 0.0 neutron star and black hole retention set. Left: HST range. Right: All bounds stars.

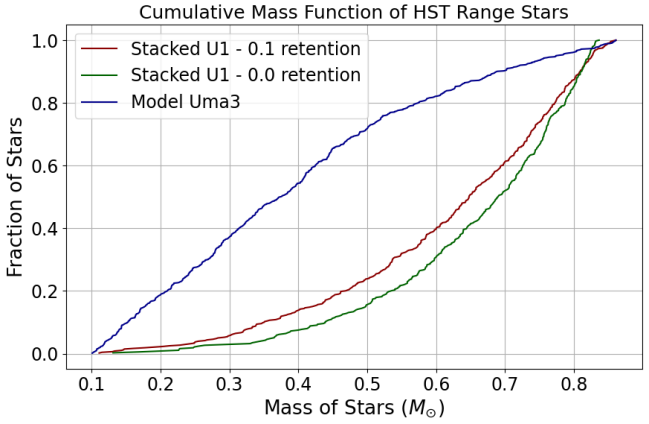


**Figure 5.** Cumulative mass function of: Stacked 0.1 retention simulations (red), stacked 0.0 retention simulations (green), UMa3 UFD model (blue)

the HST range at UNIONS time, 382 of which are in the UNIONS range.

While several studies estimate the effects of tidal stripping of stars and dark matter from UFDs (Peñarrubia et al. 2008; Errani et al. 2018; Fattahi et al. 2016), it is well-documented that UFDs are among the most dark matter-dominated Milky Way satellites, making them highly resistant to tidal stripping (Simon 2019; Errani et al. 2015; Belokurov et al. 2007; Simon & Geha 2007; Willman 2010). Given that UMa3/U1 is the smallest known UFD candidate, and since the size and luminosity of UFDs are inversely correlated with their mass-to-light ratios (Simon & Geha 2007; Wolf et al. 2010; Martin et al. 2008), we expect minimal stellar loss. Even if some stars are lost, the lack of mass segregation in dark matter-dominated systems means that this loss would not significantly alter the overall mass function, and UMa3's present-day mass function should closely resemble its initial mass function. We therefore create a model UMa3 UFD by randomly sampling from a Baumgardt et al. (2023) initial mass function described in 2.2, until it has in the UNIONS range the same number of stars as the stacked 0.1 retention simulations have in the UNIONS range, 382. We did a similar comparison for each individual star cluster model, creating UMa3 UFD present-day mass function models by randomly sampling each cluster's initial mass function. Out of twenty simulations, a significant difference ($p$ value less than 0.05) was observed in nineteen, when counting stars within the HST range, and thirteen when counting stars within the UNIONS range (Table 1 and 2 ).

### 6.1 Mass Function: Results and Conclusion

The cumulative mass function plot, figure 5 clearly shows a significant difference in the mass functions of the UMa3 UFD model and the stacked U1 models. Comparing the stacked 0.1 retention models to the UFD model, the KS statistic is 0.52 and the p-value is $1.16 \times 10^{-71}$. Comparing the stacked 0.0 retention models to the UFD model, the KS statistic is 0.60 and the p-value is $4.35 \times 10^{-84}$. Just taking the least significant of the two results gives a significance level of $\sigma = 18.42$. This highly significant result, leads us to to conclude that present day mass function can be used by future observers looking to classify UMa3/U1 as either a UFD or self gravitating star cluster. More broadly we propose that present day mass function may be used to assist the classification of other small faint milky way satellites.

## 7 SUMMARY

Errani et al. (2024) argue that if UMa3/U1 were a star cluster, its low density would cause it to rapidly disintegrate due to tidal interactions with the Milky Way's gravitational potential. Using the collisionless particle-mesh code SUPERBOX (Fellhauer et al. 2000), they demonstrate that UMa3/U1 could not survive much longer than 0.4 Gyr as a star cluster without dark matter. Given its proposed age of approximately 12 Gyr (Smith et al. 2024), the likelihood of observing UMa3/U1 just before its demise is low, leading them to conclude that UMa3/U1 is more likely a UFD, protected by its dark matter halo.

However, the collisionless code used by Errani et al. (2024), which softens interstellar forces, may underestimate the influence of massive but invisible remnants within the cluster, thus affecting the derived lifetime of U1. While SUPERBOX is computationally efficient for sparsely populated systems, it is less accurate for globular clusters where close stellar encounters are common. By using the collisional N-body code NBODY7 (Nitadori & Aarseth 2012) we accurately model close encounters, binary interactions, and stellar collisions. Our simulations predict a significantly longer survival time for UMa3/U1 as a star cluster, suggesting it is not unlikely to observe it in its current state. This strengthens the possibility that UMa3/U1 could still be a star cluster rather than a UFD. By incorporating a novel method to calculate the cluster's density center and tidal radius, as described in 2.4, our study challenges previous claims and supports the notion that multi-epoch spectroscopy is needed to definitively confirm its nature.

Our N-body simulations also show the following:

(i) A high value and variability in velocity dispersion, with a mean velocity dispersion, $\sigma = 1.3$ km/s $\pm$ 1.6 km/s, affirming that the velocity dispersion calculated by Smith et al. (2024) for UMa3/U1 candidate stars, 3.7 km/s $\pm$ 1.614 km/s, is not inconsistent with a star cluster classification.

(ii) If UMa3/U1 is a star cluster, it would exhibit significant mass segregation. However, it is unlikely that UNIONS or even deeper photometric surveys will be able to observe this due to their inability to detect remnant stars.

(iii) Present day mass function is a powerful tool for classifying systems like UMa3/U1, with potential for broader application. This approach is novel and was not used in Errani et al. (2024) for determining UMa3/U1's nature.

## 8 DISCUSSION

In Appendix A Errani et al. (2024) revise their earlier time to dissolution estimate headlined in their abstract and summary, by accounting for observational uncertainties in the present position and velocity of UMa3/U1 and using an alternate milky way potential model. Using the SUPERBOX code with the Bovy potential a survival time of approximately 1.4 Gyr is obtained, more akin to our findings. This shows significant variability can be obtained by altering the start position and potential of a cluster orbit.

As discussed in Section 4.1, selection effects may have been introduced in our 0.1 retention simulations due to a preference for simulations falling below our 10 Gyr age lower threshold rather than above our 14 Gyr age upper threshold. Although none of these simulations were included in the final analysis, this suggests that the chosen progenitor size of $n = 7200$ was too low. It would be difficult to analyze the effect of this statistical imbalance, but if someone were to rerun the simulations, we would suggest exploring sizes above $n = 7200$.

Whilst elliptical tidal radius formulas exist, we chose to use the

circular tidal radius formulae 2 keeping $V_g$ and $R_g$ updated for each time step (see section 2.4). We did this because it is not clear which elliptical formulae is most accurate to reality. If further work makes it clear that an elliptical formulae is accurate and robust, our analysis could be rerun with that tidal radius formulae.

## ACKNOWLEDGEMENTS

SMS acknowledges funding from the Australian Research Council (DE220100003). Parts of this research were conducted by the Australian Research Council Centre of Excellence for All Sky Astrophysics in 3 Dimensions (ASTRO 3D), through project number CE170100013.

## DATA AVAILABILITY

The data used in this study is available upon request by emailing the first author.

## REFERENCES

Almeida J. S., Trujillo I., Plastino A. R., 2024, The stellar distribution in ultra-faint dwarf galaxies suggests deviations from the collision-less cold dark matter paradigm (arXiv:2407.16755), https://arxiv.org/abs/2407.16755
Amôres E. B., et al., 2021, Monthly Notices of the Royal Astronomical Society, 508, 1788
Banerjee S., Belczynski K., Fryer C. L., Berczik P., Hurley J. R., Spurzem R., Wang L., 2020, A&A, 639, A41
Baumgardt H., Sollima A., Hilker M., 2020, Publ. Astron. Soc. Australia, 37, e046
Baumgardt H., Faller J., Meinhold N., McGovern-Greco C., Hilker M., 2022, MNRAS, 510, 3531
Baumgardt H., Hénault-Brunet V., Dickson N., Sollima A., 2023, MNRAS, 521, 3991
Belokurov V., et al., 2007, The Astrophysical Journal, 654, 897
Binney J., Tremaine S., 1987, Galactic Dynamics, 1st edn. Princeton University Press, Princeton, NJ
Bode P., Ostriker J. P., Turok N., 2001, ApJ, 556, 93
Bovy J., 2015, ApJS, 216, 29
Bressan A., Marigo P., Girardi L., Salasnich B., Dal Cero C., Rubele S., Nanni A., 2012, MNRAS, 427, 127
Casertano S., Hut P., 1985, ApJ, 298, 80
Cerny W., et al., 2023, ApJ, 953, 1
Errani R., Peñarrubia J., Tormen G., 2015, Monthly Notices of the Royal Astronomical Society, 449, L46
Errani R., Peñarrubia J., Walker M. G., 2018, Monthly Notices of the Royal Astronomical Society, 481, 5073
Errani R., Navarro J. F., Smith S. E. T., McConnachie A. W., 2024, ApJ, 965, 20
Fattahi A., et al., 2016, Monthly Notices of the Royal Astronomical Society, 457, 844
Fellhauer M., Kroupa P., Baumgardt H., Bien R., Boily C. M., Spurzem R., Wassmer N., 2000, New Astronomy, 5, 305
Fryer C. L., Belczynski K., Wiktorowicz G., Dominik M., Kalogera V., Holz D. E., 2012, The Astrophysical Journal, 749, 91
Giersz M., Heggie D. C., 1994, Monthly Notices of the Royal Astronomical Society, 268, 257
Hernquist L., 1990, The Astrophysical Journal, 356, 359
Hilker M., Baumgardt H., Infante L., Drinkwater M., Evstigneeva E., Gregg M., 2007, A&A, 463, 119
Hobbs G., Lorimer D. R., Lyne A. G., Kramer M., 2005, MNRAS, 360, 974
Hurley J. R., Pols O. R., Tout C. A., 2000, MNRAS, 315, 543
Kim D., Jerjen H., Mackey D., Da Costa G. S., Milone A. P., 2016, ApJ, 820, 119
King I., 1962, AJ, 67, 471
Kroupa P., 2001, MNRAS, 322, 231
Krumholz M. R., McKee C. F., Bland-Hawthorn J., 2019, ARA&A, 57, 227
Kustaanheimo P., Stiefel E., 1965, J. Reine Angew. Math., 218, 204
Martin N. F., de Jong J. T. A., Rix H. W., 2008, The Astrophysical Journal, 684, 1075
McConnachie A. W., Côté P., 2010, ApJ, 722, L209
Mikkola S., Aarseth S. J., 1989, Celestial Mechanics and Dynamical Astronomy, 47, 375
Mikkola S., Aarseth S. J., 1993, Celestial Mechanics and Dynamical Astronomy, 57, 439
Miyamoto M., Nagai R., 1975, Publications of the Astronomical Society of Japan, 27, 533
Munshi F., Brooks A. M., Christensen C., Applebaum E., Holley-Bockelmann K., Quinn T. R., Wadsley J., 2019, The Astrophysical Journal, 874, 40
Navarro J. F., Frenk C. S., White S. D. M., 1997, The Astrophysical Journal, 490, 493
Nitadori K., Aarseth S. J., 2012, MNRAS, 424, 545
Peñarrubia J., McConnachie A., Navarro J. F., 2008, Monthly Notices of the Royal Astronomical Society, 383, 247
Press W. H., Teukolsky S. A., Vetterling W. T., Flannery B. P., 1992, Numerical Recipes in C: The Art of Scientific Computing. Cambridge University Press
Salpeter E. E., 1955, The Astrophysical Journal, 121, 161
Schlegel D. J., Finkbeiner D. P., Davis M., 1998, ApJ, 500, 525
Schönrich R., Binney J., Dehnen W., 2010, MNRAS, 403, 1829
Shapiro S. S., Wilk M. B., 1965, Biometrika, 52, 591
Simon J. D., 2019, Annual Review of Astronomy and Astrophysics, 57, 375–415
Simon J. D., Geha M., 2007, The Astrophysical Journal, 670, 313
Smith S. E. T., et al., 2024, ApJ, 961, 92
Spitzer L., 1987, Dynamical Evolution of Globular Clusters. Princeton University Press, Princeton
Willman B., 2010, Advances in Astronomy, 2010, 1
Willman B., Geha M., Strader J., Strigari L. E., Simon J. D., Kirby E., Ho N., Warres A., 2011, AJ, 142, 128
Wolf J., Martinez G. D., Bullock J. S., Kaplinghat M., Geha M., Muñoz R. R., Simon J. D., Avedo F. F., 2010, MNRAS, 406, 1220

This paper has been typeset from a TEX/LATEX file prepared by the author.